EXPERIMENTAL STUDY ON THE DYNAMICS OF HOLE-PIERCING MECHANISM OF DEFORMABLE GEARS

Jinlong FENG [1,2,3], Shujuan YI [1*], Qichao LI [3]

The hole pricking mechanism is a key part of deep-fertilization liquid fertilizer applicator as well as the major source of vibration of a working applicator. A dynamic characteristic test bench of the hole pricking mechanism was developed to obtain the dynamic characteristics of the mechanism. Based on the test bench, the sun gear torque and the soil reactive force exerted on the pricking spray fertilizer needle were measured through torque sensor, signal collector and DASP-10 software. Then, with the torque applied to the sun gear and the soil reactive force exerted on the pricking spray fertilizer needle as the test indexes and the soil-bin trolley velocity, planet carrier speed and fertilization depth as the test factors, dynamic characteristics tests were performed using central composite rotatable design (CCRD) method. Relationship models between the testing factors with the sun gear torque and the soil reactive force exerted on the pricking spray fertilizer needle were constructed, and multi-objective optimization and test verification were carried out on the torque and soil reactive force. The optimal results were: trolley velocity: 0.56m/s; planet carrier speed: 62rpm; pricking depth: 120mm. Verification test results showed a good consistency between the predicted results and the test results, which provides a theoretical basis for the dynamic analysis of deep-fertilization liquid fertilizer applicator.

Keywords: hole pricking mechanism; dynamic analysis; torque; tension-compression; variance analysis; CCRD

1. Introduction

Recently, deep-fertilization liquid fertilizer applicators with high fertilizer efficiency and utilization have received wide recognitions with the promotion and popularization of liquid fertilizer. As a key part of deep-fertilization liquid fertilizer applicator, the pricking hole mechanism is an executive component to apply the liquid fertilizer into the deep soil, which is also the major source of

[1] College of Engineering, Heilongjiang Bayi Agricultural University, Heilongjiang Daqing 163319, China
[2] Quality Supervision and Testing Center for Agricultural Processed Products of the Ministry of Agriculture (Daqing), Heilongjiang Daqing 163319, China
[3] College of Mechanical and Electrical Engineering, Lingnan Normal University; Zhanjiang 524048, China
* Corresponding author: hahabodd798@163.com

vibration during the operation of the fertilizer. The performance of the pricking hole mechanism has direct effect on the quality and efficiency of fertilization operationsr [1,2]. Well-behaved pricking hole mechanism can better deal with the impact of soil and improve the reliability and service life of the mechanism.

There have been no studies on the pricking hole mechanism of deep-fertilization liquid fertilizer applicator in foreign countries. As in China, Literature [3-9]. raised four types of pricking hole mechanisms, namely crank rocker, planetary elliptic gears, all planetary elliptic gears and non-circular planetary gear trains, and kinematics analyses and simulations, structure optimization and bench tests have been conducted on the four mechanisms. The optimized or transformed mechanism can already meet the agronomic requirements of deep-fertilization of liquid fertilizer. However, the problems of large pricking inertia, unstable pricking and obvious vibrations were also reported, which further influenced the quality and efficiency of the pricking and fertilization. In the conditions that the speeds of machine and planet carrier satisfy the working requirements and the fertilization depth satisfies the agronomic requirements, the quality of fertilization mainly embodies in small hole, less fertilizer consumption and little vibrations.

Deformed gears have the feature of non-uniform transmission. By adjusting the deformation coefficient and eccentricity ratio, the deformed gears can realize a two-way variation of transmission ratio in both horizontal and vertical directions, which can increase the adjustable range of transmission ratio. Using deformed gears as the transmission part on rotary pricking hole mechanism can form a new pricking hole mechanism with small hole and high perpendicularity to the soil.

In this paper, the hole-piercing mechanism of deformable gears of liquid fertilizer injection type is taken as the research object. When the mechanism is working, the sun-gear shaft torque and the soil reaction force experienced by the fertilizer spraying needle when it enters the soil are the main factors that affect the hole-piercing trajectory, posture and machine vibration of the fertilizer spraying needle [10]. Hence, this paper takes the research objects of the sun-gear shaft torque and the soil reaction force when the fertilizer spraying needle enters the soil and uses experimental research to measure and test the dynamic parameters on the designed dynamic characteristics test bench. A torque sensor is used to obtain the torque value of the sun-gear shaft, and a strain sensor and data processing software are employed to obtain the magnitude of the soil reaction force acting on the fertilizer spraying needle when it enters the soil. Using the test objects of the torque value and the reaction force of the fertilizer spraying needle into the soil, taking the speed of the trolley, the speed of the planet carrier and the depth of fertilization as the test factors, and using a central composite rotatable design, this paper analyzes the variation of main vibration sources of the mechanism and optimizes the work parameters to improve the hole-piercing

quality and efficiency of the fertilizer applicator, in the hope of providing theoretical value for the improvement and strength analysis of the hole-piercing mechanism.

2. Materials & Methods

2.1. Structure and Working Principle of Pricking Hole Mechanism

Fig. 1 shows the structure of liquid fertilizer injection pricking hole mechanism with deformed gears, which mainly consists of five congruent deformed gears, one planet carrier, one pair of rocker arms and spray fertilizer needles. Two pairs of deformed gears are arranged at the two sides of the long shaft of central deformed solar gear. The central deformed gear is coaxially arranged with the planet carrier. The planetary gear is consolidated with the rocker arm, and the spray fertilizer needle is fixed on one end of the rocker arm. The central deformed solar gear (6) transfers the power to the intermediate deformed gears(5) and (7) which convey the power through gear engagement to the deformed gears (4) and (8), and finally to the spray fertilizer needle. When the mechanism is working, the central deformed solar gear (6) stays fixed, the planet carrier rotates, the two intermediate deformed gears revolves around the central deformed solar gear (6) and drives the spray fertilizer needles for hole pricking, each rotation pricking two holes.

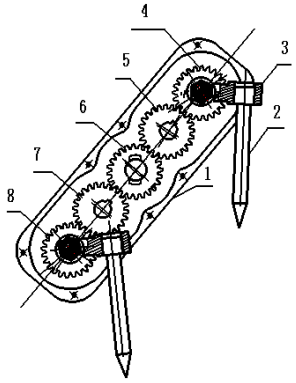

1. Planet carrier; 2. Spray fertilizer needle; 3. Rocker arm; 4. Upper planetary deformed gear; 5. Upper intermediate deformed gear; 6. Deformed solar gear; 7. Lower intermediate deformed gear; 8. Lower planetary deformed gear

Fig. 1. Structure of pricking hole mechanism

2.2. Dynamic Test Bench of Liquid Fertilizer Injection Pricking Hole Mechanism with Deformed Gears

2.2.1. Test parameters and test methods of test bench

The pricking hole mechanism connects with other parts of deep-fertilization liquid fertilizer applicator with chain drive to complete the deep-

fertilization, which is the major source of vibration during the operation of the liquid fertilizer applicator. The major cause to the vibration during working is the torque produced as the chain drives the solar axle and the soil reactive force exerted on the pricking spray fertilizer needles. To better understand the dynamic characteristics of the pricking hole mechanism during working, the solar gear torque and the soil reactive force exerted on the pricking spray fertilizer needle were used as the test parameters of the test bench.

The solar gear torque was obtained from torque sensor, and the soil reactive force exerted on the pricking spray fertilizer needle (tension-compression) was calculated by the micro strain through the strain gauge attached on the root of the spray fertilizer needle.

2.2.2. Structure and test principle of dynamic test bench

A matching test bench was designed according to the dynamic parameters to be tested. Through test analysis, the study aimed to provide theoretic basis for further research on the pricking hole mechanism. Fig. 2 shows the designed test bench platform, which consists of the test bench, the torque sensor, the pricking hole mechanism with deformed gears, the strain regulator, the signal collector, and the tacho-torquemeter. The operation of the test bench was realized by controlling two motors on the test bench through a variable frequency drive cabinet. One motor controls the reciprocating movement of the test bench on the soil-bin guide rail, and the other motor controls the rotation of the pricking hole mechanism through a gear actuator, each rotation pricking two holes. The depth of the mechanism is controlled by changing the length of the spray fertilizer needle.

1. Test bench; 2. Torque sensor; 3. Pricking hole mechanism;
4. DASP-10 software; 5. Tacho-torquemeter; 6. Strain regulator; 7. Signal collector

Fig. 2. Test bench of dynamic test platform

The solar gear torque can be directly measured by JN338A dynamic torque sensor and the matching torque and speed measuring instrument. The force exerted on the pricking spray fertilizer needles was collected through strain sensor, which was then converted into electrical signals or other required information forms according to a certain law. This test adopted a strain sensor that

can convert strain into resistance and used half bridge measurement method to test the soil reactive force exerted on the pricking spray fertilizer needle, that is, the tension-compression in parallel with the spray fertilizer needle.The type of strain gauge used in this test is BX120-0.5AA. During the test, the strain gauge sensor was attached to the cylindrical surface near the root of the spray fertilizer needle. When the pricking hole mechanism enters the soil, slight deformation would happen to the spray fertilizer needles. At this time, the strain gauge sensor would transmit the voltage signals to the dynamic strain meter, and the signal collector would convert the voltage signals received by the dynamic strain meter into digital signals. After pretreatments such as signal amplification and combination with DASP-10 software for signal collector, we can obtain the tension-compression strain changes of the spray fertilizer needles during the whole hole pricking process. Then calibration test was performed to analyze the relationship between the tension-compression strain with the force applied on the spray fertilizer needles, and further obtain the soil reactive force exerted on the pricking spray fertilizer needles [11-15].

2.3. Dynamic Characteristic Tests

2.3.1. Test equipment and test conditions

Test equipment include dynamic test bench of pricking hole mechanism, liquid fertilizer injection pricking hole mechanism with deformed gears, INV1861A portable strain regulator, INV3018C signal collector produced by China Orient Institute of Noise & Vibration and the matching DASP-10 software, JN338A dynamic torque sensor and the matching tacho-torquemeter.

The self-built soil bin laboratory of Northeast Agricultural University was chosen as the test site. The length of the soil bin was 12m; the distance between two guide rails was 1.7m; black loam soil was used and put in the soil bin; according to the requirement of soil condition during the intertillage, the soil hardness was set as 0.6MPa-1MPa and water content 20%-25%.

2.3.2. CCRD test design

Based on the single-factor test, a three-factor, five-level CCRD method [16-17] was adopted to determine the value ranges of the influencing factors: 0.55-0.65m/s for the forward velocity of test trolley, 60-80 rpm for the planet carrier speed, and 110-130 mm for the pricking depth. Table 1 shows the test plan and results of three-factor, five-level CCRD method.

Table 1

CCRD test plan and results

Test number	Trolley velocity x_1	Speed of planet carrier x_2	Pricking depth x_3	Torque y_1	Strain y_2
1	0.55	60	110	3.07	8.15
2	0.65	60	110	4.56	7.07
3	0.55	80	110	5.23	7.59
4	0.65	80	110	8.52	6.33
5	0.55	60	130	6.78	7.54
6	0.65	60	130	7.24	7.11
7	0.55	80	130	7.92	8.41
8	0.65	80	130	8.81	7.36
9	0.52	70	120	4.42	7.61
10	0.68	70	120	8.32	6.67
11	0.60	53	120	5.06	7.29
12	0.60	87	120	9.12	7.58
13	0.60	70	103	7.72	6.39
14	0.60	70	137	7.63	7.19
15	0.60	70	120	7.72	6.85
16	0.60	70	120	7.53	6.83
17	0.60	70	120	7.84	6.86
18	0.60	70	120	7.82	6.84
19	0.60	70	120	7.85	6.83
20	0.60	70	120	7.42	6.84
21	0.60	70	120	7.52	6.88
22	0.60	70	120	7.63	6.83
23	0.60	70	120	7.52	6.84

3. Results and Discussion

Absolute prediction error ε_{AME} and the root mean square error of prediction ε_{RSME} can be calculated by following formulas [18].

$$\varepsilon_{AME} = \frac{1}{p}\sum_{i=1}^{p}\left(\frac{\left|y_{ie} - y_{ip}\right|}{y_{ie}} \times 100\%\right) \tag{1}$$

$$\varepsilon_{RSME} = \left[\frac{1}{P}\sum_{I=1}^{P}(y_{ie} - y_{ip})^2\right]^{1/2} \tag{2}$$

where, p is the number of test groups; y_{ie} represents the test data; y_{ip} refers to the predicted value corresponding to the test data; i refers to the 0-p variables.

3.1. Variance Analysis of Torque

The variance analysis results of the influence of test factors on the solar gear torque were shown as Table 2. According to the variance analysis (ANOVA),

we conclude that: the test statistical F-value followed by torque model was 10.17; P-value can be used to inspect the reliability of the modeling; it is generally assumed that P-value=0.05 is a boundary level for acceptable errors; obviously, the P-value of the torque model is smaller than 0.0001, indicating a significant model; R2 is the determination coefficient of the model, which refers to the degree of fitting of the model; R_2=0.9156, which means that less than 9% of the total variation in the torque model cannot be explained; PA represents the signal-to-noise ratio of the model; PA>4 means that the established model is satisfactory; the torque model PA=12.55 means that the established model is significant; R_P^2 refers to the accuracy of the model in predicting new data; the torque model R_P^2=0.879 also means the established model is significant. The second order polynomial model of the torque is expressed as following:

Table 2

Variance analysis of torque

Item	Quadratic sum SS	Degree of freedom DOF	Mean square MS
Model	45.9	9	5.1
Residual	6.52	13	0.50
Pure error	0.21	8	0.026
Sum	52.44	22	
R2 0.915	PA Rp2 12.55 0.879	F-value 10.17	P-value 0.0001

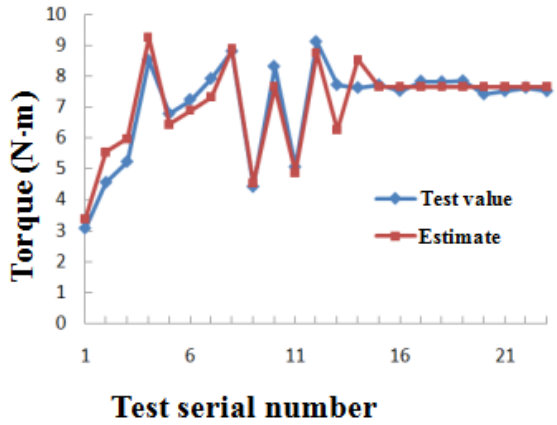

Fig. 3. Comparison between test results and predicted results of torque

$$y_1 = -201.724 + 348.655x_1 + 0.712x_2 + 1.104x_3 + 0.558x_1x_2 - 0.86x_1x_3 - 0.004x_2x_3 - 221.83x_1^2 - 0.003x_2^2 - 0.001x_3^2 \quad (3)$$

Constraints: 0.52m/s≤x1≤0.68m/s; 53rpm≤x2≤87rpm; 103mm≤x3≤137mm

The absolute mean prediction error and root-mean-square error of the solar axle torque model were calculated through Formula (1) and Formula (2), which were 5.01% and 0.531, respectively. Fig. 3 shows certain difference between the test results and predicted results of the torque model due to the deviation of the model in the prediction. But the model can provide a satisfactory prediction of the torque parameters.

3.2. Variance analysis of tension-compression

Table 3 shows the results of the variance analysis (ANOVA) of the impact of the tension-compression exerted on the pricking spray fertilizer needle. As shown, the test statistical F-value followed by tension-compression model was 14.55; the P-value of the tension-compression model is smaller than 0.0001, indicating a significant model; the model determination coefficient R2= 0.90972, which means that less than 9% of the total variation in the tension-compression model cannot be explained; the signal-to-noise ratio PA=15.08 and R_P^2=0.847 also indicate a significant tension-compression model. The second order polynomial model of the tension-compression exerted on the pricking spray fertilizer needle is expressed as following:

$$y_2 = 85.534 - 100.374x_1 - 0.622x_2 - 0.428x_3 + 0.2x_1x_2 + 0.215x_1x_3 + 0.003x_2x_3 + 67.221x_1^2 + 0.003x_2^2 + 0.001x_3^2 \quad (4)$$

Constraints: 0.52 m/s≤x1≤0.68m/s; 53rpm≤x2≤87rpm; 103mm≤x3≤137mm

The absolute mean prediction error and root-mean-square error of the tension-compression model were calculated through Formula (1) and Formula (2), which were 1.41% and 0.151, respectively. Fig. 4 shows slight difference between the test results and predicted results of the tension-compression model, which presented good consistency. This means that the established tension-compression model can reflect the internal law between the tension-compression with the trolley velocity, planet carrier speed and pricking depth.

Table 3

Variance analysis of tension-compression

Item	quadratic sum SS	Degree of freedom DOF	Mean square MS
Model	5.20	9	0.58
Residual	0.52	13	0.04
Pure error	0.0022	8	0.0003
Sum	5.71	22	
R2	PA Rp2	F-value	P-value
0.9097	15.08 0.847	14.55	<0.0001

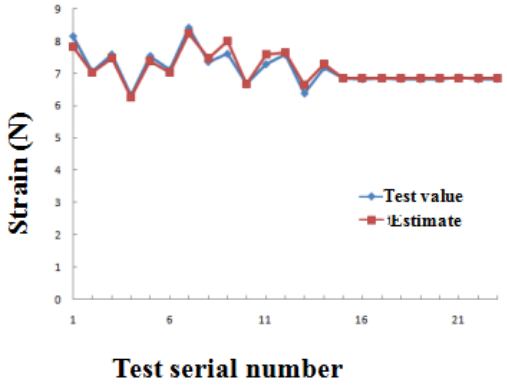

Fig. 4. Comparison of the test results and predicted results of tension-compression

3.3. Analysis of Model Interaction Items

In order to intuitively analyze the relationship between the test indexes of torque, tension-compression and other factors, the response surfaces of factor interactions were obtained using Design-Expert 8.0.5 software, as shown in Fig. 5 and Fig. 6.

Fig.5a shows that the torque increases with the increase of the trolley velocity and planet carrier speed, and decreases with the decrease of the two factors. When the trolley velocity is fixed, the torque would increase with the increase of the planet carrier speed. According to the interactions between the torque with the trolley velocity and planet carrier speed, the planet carrier speed showed greater impact on the torque than trolley velocity.

Fig. 5b shows that both the trolley velocity and pricking depth presented greater impact on the torque. When the trolley velocity is fixed, the torque would increase with the increase of the pricking depth. According to the interactions between the torque with the trolley velocity and pricking depth, the planet carrier speed presented greater impact on the torque than the pricking depth.

Fig. 5c shows that when the planet carrier speed is fixed at the level of 0, the deeper the pricking, the larger the torque. When the pricking depth is fixed, the torque would increase with the increase of the planet carrier speed. Hence, the planet carrier speed had larger impact on the torque compared with the pricking depth.

Fig. 6a shows that the higher the trolley velocity, the smaller the tension-compression; the higher the planet carrier speed, the smaller the tension-compression; according to the interactions of the tension-compression with the trolley velocity and the planet carrier speed, the trolley velocity presented larger impact on the tension-compression compared with the planet carrier speed.

Fig. 6b shows that the higher the trolley velocity, the smaller the tension-compression; the deeper the pricking, the larger the tension-compression;

according to the interactions of the tension-compression with the trolley velocity and the pricking depth, the trolley velocity presented larger impact on the tension-compression compared with the pricking depth.

Fig. 6c shows that the higher planet carrier speed, the smaller the tension-compression; the deeper the pricking, the larger the tension-compression; according to the interactions of the tension-compression with the planet carrier speed and the pricking depth, the pricking depth presented larger impact on the tension-compression compared with the planet carrier speed.

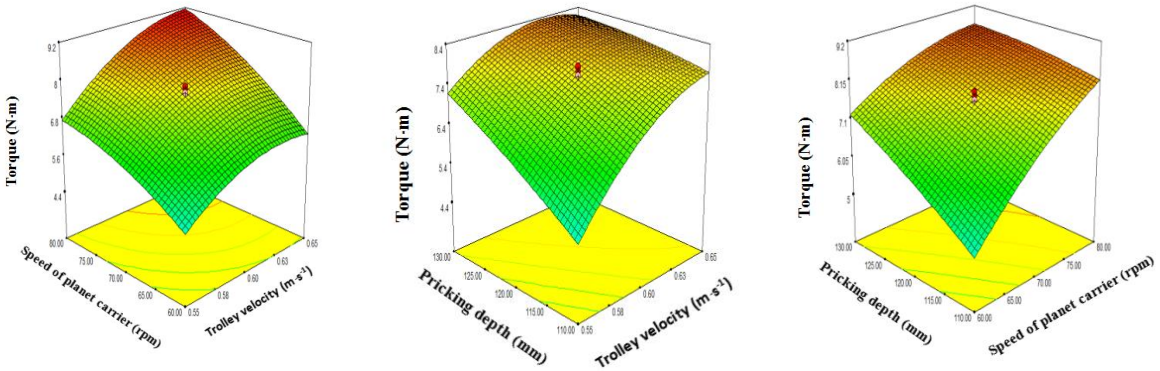

a. Interaction between trolley velocity and planet carrier speed

b. Interaction between trolley velocity and pricking depth

c. Interaction between planet carrier speed and pricking depth

Fig. 5. Response surfaces of torque

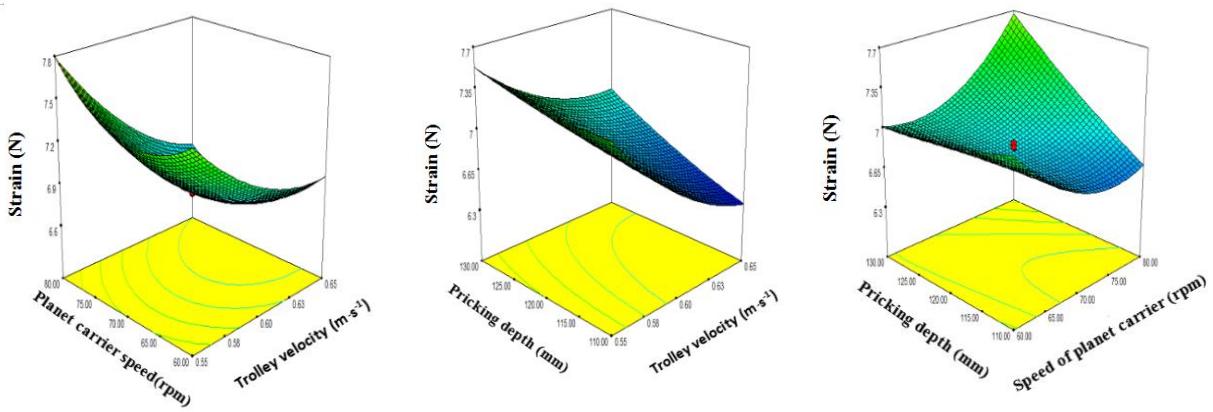

a. Interaction between trolley velocity and planet carrier speed

b. Interaction between trolley velocity and pricking depth

c. Interaction between planet carrier speed and pricking depth

Fig. 6. Response surfaces of tension-compression

3.4. Optimization and Test Verification

Based on the second order polynomial models of the torque and the tension-compression previously established, and with miny1 and miny2 as our ptimization objective, we adopted Design-Expert 8.0.5 software to optimize the

objective function and get the optimal parameter combination as follows: trolley velocity: 0.562 m/s; planet carrier speed: 62.32 rpm; pricking depth: 120.2mm. We further optimize these parameters to be: trolley velocity: 0.56m/s; planet carrier speed: 62 rpm; pricking depth: 120 mm. The torque y1 and tension-compression y2 under this optimal parameter combination were 4.11 N·m and 7.56 N, respectively.

As the optimal parameter combination does not appear in the experiment, it is necessary to perform an experiment under optimal parameter conditions. In the experiment, 5 sets of repeated experiments are performed to eliminate random errors. The maximum value of the torque test is 4.25 N·m, the maximum prediction error is 3.92%, the mean value is 4.20 N·m, the mean prediction error is 2.14%; the maximum value of the tension-compression test is 7.81 N, the maximum prediction error is 3.20%, the mean value is 7.71 N, and the mean prediction error is 1.95%. Considering the errors caused by the equipment accuracy and human operation during the tests, it is verified that the test results are close to the predicted results under the optimal parameter combination, and the good consistency indicates that the optimization model is feasible.

4. Conclusions

(1) A dynamic test bench was designed based on the liquid fertilizer injection pricking hole mechanism with deformed gears, which can satisfy the requirements of parameter test.

(2) Dynamic characteristic tests were performed using torque sensor, signal collector and DASP-10 software to measure the solar gear torque and the soil reactive force exerted on the pricking spray fertilizer needles. The impacts of trolley velocity, planet carrier speed and pricking depth on the torque and tension-compression were studied through CCRD test, followed by CCRD analysis and establishment of torque and tension-compression models. Multi-objective optimization was conducted on the torque and tension-compression. The optimized results were: trolley velocity: 0.56 m/s; planet carrier speed: 62rpm; pricking depth: 120 mm.

(3) Verification tests were conducted. The results showed a good consistency between the verification results and the predicted results under the optimal combination, which provides theoretical basis for the dynamic analysis of the deep-fertilization liquid fertilizer applicator.

Acknowledgments

Thank you for Postdoctoral Science Foundation of Heilongjiang Province of China (Grant No. LBH-Z18254), Heilongjiang Bayi Agricultural University Support Program for San Heng San Zong (TDJH201803)

REFERENCES

[1]. *Marcelo J. da Silva, Paulo S.G. Magalhães*. A liquid injection dosing system for site-specific fertiliser management. 2017, 163: 150-158.
[2]. *Jagvir Dixit, Vinay Kumar, Mudasir Ali*. Development and Evaluation of a Single Row Manual Vegetable Transplanter. 2018, 42(2): 58-66.
[3]. *Zhou Changjiang , Hu Bo , Chen Siyu , et al*. Design and analysis of high-speed cam mechanism using Fourier series. 2016, 104: 118-129.
[4]. *Zhang Lingbo , Cai Zongxi , Wang Liwei , et al*. Coupled Eulerian-Lagrangian finite element method for simulating soil-tool interaction. 2018, 175: 96-105.
[5]. *Zhang L.B. , Z.X. Cai, H.F. Liu*. A novel approach for simulation of soil-tool interaction based on an arbitrary Lagrangian–Eulerian description. 2018, 178: 41-49.
[6]. *WANG Jinwu, Zhou Wenqi, BAI Haic, hao, et al*. Design and experiment of differential ype bi directional distribution device for fertilizer supply for deep-ertilizer liquid fertilizer application. Transactions of the Chinese Society for Agricultural Machinery, 2018, 49(6): 106-111.
[7]. *Wang Jinwu, Liu Y, Wang J, and He J*. Optimized design and experimental of the liquid fertilizer deep mechanism with planetary elliptic gears. Transactions of the Chinese Society for Agricultural Machinery, 2012, 43(10), 59–65.
[8]. *Wang Jinwu, Zhou Wenqi, Wang X, Li X, and Wang J*. Oblique type pricking hole mechanism based on lagrange curve for cubic fitting trajectory. Transactions of the Chinese Society for Agricultural Machinery, 2017, 48(5), 79–85.
[9]. *Wang Jinwu, Wang J, Ju J, and He J*. Research progress on pricking hole mechanism of deep-fertilization liquid fertilizer applicator. Journal of Northeast Agricultural University, 2013, 44(2), 157–160.
[10]. *Wang Jinwu, Wang J, and Ju J*. Dynamics optimization for pricking hole mechanism of deep-fertilization liquid fertilizer applicator. Transactions of CSAE, 2011, 27(1), 165–169.
[11]. *Chen J, Li Ge, and Zhao Y*. Study of dynamic characteristics of transplanting mechanism with elliptic planetary gears through experiment. Transactions of the Chinese Society for Agricultural Machinery, 2011, 37(1), 40–41,46.
[12]. *Chen Jianneng, Wang Ying, Hang Q, Hang H, Wu C, and Zang P*. Optimization and test of transplanting mechanism with planetary deformed elliptic gears for potted-seedling transplanter. Transactions of the Chinese Society for Agricultural Machinery, 2013, 44(10), 52–56,92.
[13]. *Yu Gaohong, Chen Jianneng, Zhao F, and Zhao Y*. Dynamics Analysis of Transplanting Mechanism with Planetary Spur Gears. Transaction of the Chinese Society for Agricultural Machinery, 2015, 36(4), 51–55.
[14]. *Wang Ying, Chen Jianneng, Zhon L, Li P, and Zhang G*. Dynamics Analysis and Experiment of Conjugate Cam Seedling-pushing Device Applied on Walking-rice Transplanter. Transactions of the Chinese Society for Agricultural Machinery, 2012, 3(10), 47–53.
[15]. *Ye Bingliang, Li Li, Yu Gaohong, Liu A, and Zhao Yun*. Dynamics Analysis and Test on Rotary Pick-up Mechanism for Vegetable Pot-seedling. Transactions of the Chinese Society for Agricultural Machinery, 2014, 46(6), 70–78.
[16]. *Meng Gemali*. Experimental design and analysis. Beijing, People's Posts and Telecommunications Press, 2009.
[17]. *Ren Luquan*. Experimental optimization design and analysis. Beijing, Higher Education Press, 2003.
[18]. *Xu Zhongru*. Experimental regression design. Heilongjiang Science and Technology Press, 1998.